

Adaptive Control for Marine Vessels Against Harsh Environmental Variation

Fangwen Tu, Shuzhi Sam Ge, *Fellow, IEEE*, Yoo Sang Choo, and Chang Chieh Hang, *Fellow, IEEE*

Abstract—In this paper, robust control with sea state observer and dynamic thrust allocation is proposed for the Dynamic Positioning (DP) of an accommodation vessel in the presence of unknown hydrodynamic force variation and the input time delay. In order to overcome the huge force variation due to the adjoining Floating Production Storage and Offloading (FPSO) and accommodation vessel, a novel sea state observer is designed. The sea observer can effectively monitor the variation of the drift wave-induced force on the vessel and activate Neural Network (NN) compensator in the controller when large wave force is identified. Moreover, the wind drag coefficients can be adaptively approximated in the sea observer so that a feedforward control can be achieved. Based on this, a robust constrained control is developed to guarantee a safe operation. The time delay inside the control input is also considered. Dynamic thrust allocation module is presented to distribute the generalized control input among azimuth thrusters. Under the proposed sea observer and control, the boundedness of all the closed-loop signals are demonstrated via rigorous Lyapunov analysis. A set of simulation studies are conducted to verify the effectiveness of the proposed control scheme.

Index Terms—Dynamic positioning, sea state observer, robust constrained control, input delay, dynamic thrust allocation, deep water technology

I. INTRODUCTION

FPSOs unit are highly demanded to produce, process hydrocarbons and store oil in marine industry. At the same time, Accommodation Vessels (AV) which can provide the space for logistic support and open deck space in deep sea environment is needed to handle the maintenance related work offshore. In this way, these AVs must ensure connected for continuous personnel and equipments transfer through gangway. Thus, the motivation of this paper is to design a DP system to allow the AVs to maintain proper relative position and heading under varying environmental situations.

One of the most significant phenomena during the operation is the hydrodynamic interaction between the two vessels. This strong influence is called shielding effect [1] which results in huge environmental force variation. The ocean waves can propagate in multiple directions. Once the smaller accommodation vessel situates in the downstream shadow of FPSO as shown in Fig. 1, the large FPSO would protect the smaller vessel in the vicinity. Consequently, the vessel only receives small wave-induced force. When the vessel moves out of the shadow, the environmental loads on the AV would increase. Thus, it is a very challenging to keep a fixed relative position and heading under this variation. In order to alarm the it, for the first time, a novel sea state observer is proposed. The observer is motivated by the fault diagnosis process in

fault tolerant control [2] [3]. Different from traditional fault observer, the sea state observer is able to adaptively estimate the wind force and moment. The estimated force and moment is used for a feedforward control to counteract the wind effect on the vessel. Based on this, the detection of the shielding effect is not only judged by the residual between actual system states and estimated states, but, the estimated wind drag coefficients are selected as the indicator of the shielding effect due to the over-estimation phenomena. After huge wave-induced force and moment are detected, NNs are applied in both sea observer and controller to compensate the wave force.

Additionally, to ensure the extended length of gangway

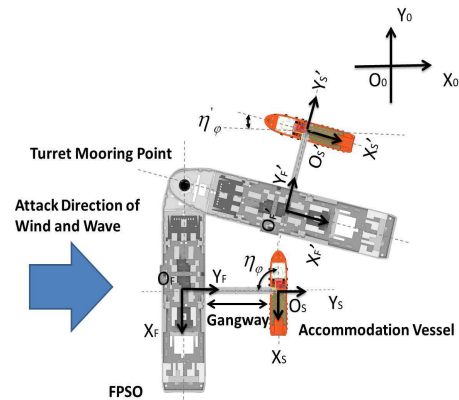


Fig. 1. Definition of the coordinate system

between an AV and the FPSO not exceed the limit stroke, the tracking errors must be regulated. In [4], Barrier Lyapunov Function (BLF) method was proposed to handle output constraint. Compared to other schemes, BLF needs less restrictive initial conditions and does not require the explicit system solution. A general framework to handle the prescribed performance tracking problem for strict feedback systems were proposed in [5]. Apart from tracking error constraint, the input delay existing in the thrusters can severely degrade the control performance. The delay is mainly caused by the long response time of the thruster driver [6]. Thus, it is necessary to take the input delay into consideration for the control design. Much research has been done to cope with input delay for linear system [7] [8]. However, the nonlinearity of the vessel systems bring more challenges to the control design. In [9] [10], an adaptive tracking control scheme has been developed for a class of multi-input and multi-output (MIMO) nonlinear system with input delay. A virtual observer is constructed as an auxiliary system to convert the input delay system into

a non-delayed one. A robust saturation control approach for vibration suppression of building structures with input delay is presented in [11]. This control is able to handle bounded time-varying input delay. But integrating tracking error constraint with input delay is seldom studied, especially for nonlinear systems. Therefore, in this paper, in order to guarantee a smooth and safe operation, both of these two requirements need to be considered simultaneously.

In this paper, we consider an AV with 6 azimuth thrusters which can produce forces in all directions. The aim of thrust allocation module is to distribute the desired control effort among the thrusters, i.e., to solve the required rotation angle and output thrust for each thruster. The overactuated propelling system makes an optimization problem. In reality, dynamic allocation is needed since the formulation of the optimization problem depends on the earlier allocation results. Moreover, due to the deployment of azimuth thrusters, the optimization problem becomes a nonconvex one [12]. Therefore, it is hard to utilize the traditional iterative numerical optimization method to search the solution. Since we always hope to search the optimal solution in the neighborhood of current thruster state (i.e. rotated angle and produced thrust), a method of local linearization [13] is proper and applicable to convert the nonconvex problem into a local convex one. Sequently, various methods such as linear programming [14] and NN dynamic solvers can be applied [15]. Although thrust allocation problem have been extensively researched, few research results are available to combine thruster-thruster interaction and other thruster property constraints together. In this manner, a more intact dynamic characteristic of the thruster is considered. The block diagram of the overall DP system can be found in Fig. 2.

The contributions of this paper is three-fold.

- (i) A novel model-based adaptive sea state observer is developed to alarm the huge environmental force variation and at the same time adaptively approximate the wind force and moment for feedforward compensation.
- (ii) Robust adaptive control is proposed in combination with predictor-based method and symmetric BLF to handle constant control input delay and output tracking error constraints simultaneously. In addition, NN is employed for the compensation of force variation.
- (iii) Both thruster-thruster interaction and other thruster property are considered in the thrust allocation module. After locally convex reformulation, LVI-based Primal Dual Neural Network (LVI-PDNN) solver is designed to search the optimal solution accurately.

II. PROBLEM FORMULATION

DP control is designed for FPSO-AV system operated under shielding effect as shown in Fig. 1. The global frame (X_0, O_0, Y_0) is defined with the origin fixed at a certain point on sea level. The local frame of FPSO (X_F, O_F, Y_F) is a moving coordinate system with its origin fixed at the midship point in the water line. X_F axis is the longitudinal axis which points to the stern of the ship. Y_F is the transversal axis which directs to the starboard. The body frame of AV

(X_s, O_s, Y_s) is defined very similar with that of the FPSO. Due to the turret mooring system and the exogenous environmental forces, the FPSO will make slow yaw motion about the turret pivot point. Thus, the AV is supposed to achieve corresponding plane motion and rotation to ensure a fixed relative position and orientation with FPSO. Let $\eta = [\eta_x, \eta_y, \eta_\psi]^T$ represents the earth-fixed position and heading of target vessel. The alongship, athwartship and rotational velocity are expressed by vector $\nu = [u_x, v_y, r_\psi]^T$. Referring to [16], the low frequency (LF) dynamic model of the vessel is considered as follows.

$$\dot{\eta} = J(\eta_\psi)\nu \quad (1)$$

$$M\dot{\nu} + C(\nu)\nu + D(\nu)\nu + g(\eta) = \tau(t-t_d) + \gamma(t-T)\tau_{\text{wave}} + \tau_{\text{wind}} + d \quad (2)$$

where $J(\eta_\psi)$ is the rotation matrix defined as

$$J(\eta_\psi) = \begin{bmatrix} \cos(\eta_\psi) & \sin(\eta_\psi) & 0 \\ -\sin(\eta_\psi) & \cos(\eta_\psi) & 0 \\ 0 & 0 & 1 \end{bmatrix} \quad (3)$$

$M = M_{\text{RB}} + M_A \in \mathbb{R}^{3 \times 3}$ is a known diagonal inertia matrix which is the sum of rigid body inertia and added mass. In DP control design, the inertia matrix is usually considered as a constant matrix [17] [16]. $C(\nu) = C_{\text{RB}}(\nu) + C_A(\nu)$ is the matrix of Coriolis and centripetal. $D(\nu)$ and $g(\eta)$ are the damping matrix and restoring force respectively. $d \in \mathbb{R}^3$ is the time-varying unknown external disturbance and unmodeled dynamics. $\tau(t-t_d) \in \mathbb{R}^3$ denotes the generalized control input with known constant time delay $t_d \in \mathbb{R}$. $\tau_{\text{wave}} \in \mathbb{R}^{3 \times 1}$ and $\tau_{\text{wind}} \in \mathbb{R}^{3 \times 1}$ represent the wave and wind force/moment. $\gamma(t-T)\tau_{\text{wave}}$ describes the hydrodynamic force variation with T denoting the an uncertain moment that the vessel starts to be subjected to the wave force. The function $\gamma(t-T)$ is defined as

$$\gamma(t-T) = \begin{cases} 0, & \text{if } t < T \\ \chi(t, T, t_T), & \text{if } t \geq T \end{cases} \quad (4)$$

where

$$\chi(t, T, t_T) = \begin{cases} \frac{T-t}{t_T}, & \text{if } t-T < t_T \\ 1, & \text{if } t-T \geq t_T \end{cases} \quad (5)$$

t_T represents the shielding time. The expression of wind force and moment in surge, sway and yaw are as follows [16].

$$\begin{aligned} \tau_{\text{wind}} = & \begin{bmatrix} 0.5\rho_{\text{air}}C_x \cos(\eta_\psi - \beta_w)V_w^2 A_T \\ 0.5\rho_{\text{air}}C_y \sin(\eta_\psi - \beta_w)V_w^2 A_L \\ 0.5\rho_{\text{air}}C_N \sin[2(\eta_\psi - \beta_w)]V_w^2 A_L L_v \end{bmatrix} \\ & + 0.5\rho_{\text{air}}V_w^2 \text{diag} [\cos(\eta_\psi - \beta_w)A_T, \sin(\eta_\psi - \beta_w)A_L, \\ & \sin[2(\eta_\psi - \beta_w)]A_L L_v] \begin{bmatrix} C_x \\ C_y \\ C_N \end{bmatrix} = \Pi\Phi \end{aligned} \quad (6)$$

where,

$$\Pi = 0.5\rho_{\text{air}}V_w^2 \text{diag} [\cos(\eta_\psi - \beta_w)A_T, \sin(\eta_\psi - \beta_w)A_L,$$

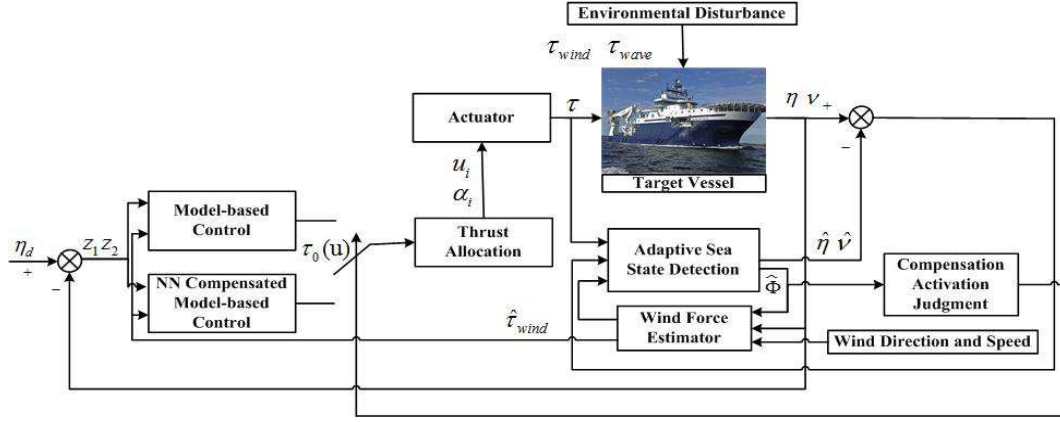


Fig. 2. Diagram of sea state observer, controller and thrust allocator

$$\sin[2(\eta_\psi - \beta_w)]A_L L_v], \Phi = \begin{bmatrix} C_x \\ C_y \\ C_N \end{bmatrix} \quad (7)$$

ρ_{air} is the density of air. Φ is the peak value of wind drag coefficient. A_T , A_L and L_v denote the transverse projected area, lateral projected area and the length of the vessel. β_w represents the attack direction of the wind. V_w is the relative velocity between the wind and the vessel. Next, we present some assumptions and remarks to facilitate the sequent development.

Assumption 1: The inertia matrix M is invertible and M^{-1} is bounded. The upper bound can be expressed as $\|M^{-1}\|_\infty \leq \bar{M}^{-1}$, where $\bar{M}^{-1} \in \mathbb{R}$ is a positive constant bound.

Assumption 2: The disturbance term d is bounded with $d^T d \leq \bar{d}$. $\bar{d} \in \mathbb{R}$ is a positive constant.

Assumption 3: In this paper, we only consider the drift wave-induced force and moment which is a low-frequency part of the wave effects. The high-frequency part is ignored.

Remark 1: Assumption 3 implies that there is no need to enclose a filter on the position and velocity signal, η and ν , during the control design.

III. ADAPTIVE SEA STATE OBSERVER

In this brief, a novel sea state observer is built to alarm the shielding effect as well as approximate the wind force and moment. To achieve this, the idea of fault detection and diagnosis is incorporated by building a model-based nonlinear observer with full state feedback. The wave-induced drift force under the shielding effect can be regarded as an evolutive fault. Large wave-induced force can be alarmed by investigating the output of the wind estimator and the residual error of the observer. In this paper, the wind and wind-generated wave force are both assumed to propagate along the X_0 direction. Initially, due to the shielding effect, the vessel is subject to the weak wind force solely. A wind drag coefficient estimator is developed to adaptively estimate the unknown peak value of wind drag coefficient Φ . When the shadow influence vanishes, the estimator would fall into overcompensation and the observation error increase. These phenomenon help us to judge the occurrence of large wave-induced force. Then, NNs which have inherent approximation capabilities [18] [19] are applied

in sea observer and the controller to encounter the uncertain wave force. The design of sea state observer is introduced in this section.

The more complicated observer after alarm with NN compensation is presented first. The formulation in (1) (2) can be rewritten into a more compact form as

$$\dot{X} = f(X)X + \phi(X) + R[\tau(t-t_d) + \gamma(t-T)\tau_{\text{wave}} + \tau_{\text{wind}} + d] \quad (8)$$

where $X = [\eta^T, \nu^T]^T$, $f(X) = \begin{bmatrix} O & J(\eta_\psi) \\ O & -M^{-1}[C(\nu) + D(\nu)] \end{bmatrix}$, $\phi(X) = \begin{bmatrix} O \\ -M^{-1}g(\eta) \end{bmatrix}$, $R = \begin{bmatrix} O \\ M^{-1} \end{bmatrix}$. Add and minus AX at the right hand side of the above expression, we obtain.

$$\dot{X} = AX + [f(X) - A]X + \phi(X) + R[\tau(t-t_d) + \gamma(t-T)\tau_{\text{wave}} + \tau_{\text{wind}} + d] \quad (9)$$

where $A^T = A \in \mathbb{R}^{6 \times 6}$ matrix is chosen to be Hurwitz and the pair (A, R) is completely controllable. According to Kalman-Yakubovich-Popov (KYP) lemma [20], there exists a symmetric matrix P and a vector Q satisfying

$$A^T P + P A = -Q Q^T \quad (10)$$

Assumption 4: $[f(X) - A]X + \phi(X)$ is Lipschitz and satisfies $\|[f(X_1) - A]X_1 + \phi(X_1) - [f(X_2) - A]X_2 - \phi(X_2)\| \leq \sigma_d \|X_1 - X_2\|$ where σ_d is Lipschitz constant.

A set of linearly parameterized NNs with Radial Basis Function (RBF) [21] is employed to handle the unknown wave force.

Consider

$$\gamma(t-T)\tau_{\text{wave}}(Z_{ow}) = W_d^{*T} S(Z_{ow}) + \epsilon \quad (11)$$

with

$$\gamma(t-T)\hat{\tau}_{\text{wave}}(\hat{Z}_{ow}) = \hat{W}_d^T S(\hat{Z}_{ow}) \quad (12)$$

we can further obtain

$$\begin{aligned} & \gamma(t-T)\tau_{\text{wave}}(Z_{ow}) - \gamma(t-T)\hat{\tau}_{\text{wave}}(\hat{Z}_{ow}) \\ &= W_d^{*T} S(Z_{ow}) - W_d^{*T} S(\hat{Z}_{ow}) + W_d^{*T} S(\hat{Z}_{ow}) \end{aligned}$$

$$\begin{aligned}
 & -\hat{W}_d^T S(\hat{Z}_{ow}) + \epsilon \\
 & = \tilde{W}_d^T S(\hat{Z}_{ow}) + W_d^{*T} [S(Z_{ow}) - S(\hat{Z}_{ow})] + \epsilon \\
 & = \tilde{W}_d^T S(\hat{Z}_{ow}) + \Lambda
 \end{aligned} \tag{13}$$

where $\hat{W}_d = \text{blockdiag}[\hat{W}_{d1}, \hat{W}_{d2}, \dots, \hat{W}_{d6}]$ is the weight matrix. W_d^* is the corresponding optimal weights and define $\tilde{W}_d = \hat{W}_d - W_d^*$. The input of the network is $Z_{ow} = [P_{\text{wave}}^T, X^T]^T$. P_{wave}^T is the wave-related measured parameters. Since the activation function is bounded, $S(Z_{ow}) - S(\hat{Z}_{ow})$ is bounded. Moreover, W_d^* and the approximation error ϵ are bounded, hence, the newly defined disturbance term $\Lambda = W_d^{*T} [S(Z_{ow}) - S(\hat{Z}_{ow})] + \epsilon$ is bounded, and it satisfies

$$\|\Lambda\|^2 \leq \bar{\Lambda} \tag{14}$$

where $\bar{\Lambda} \in \mathbb{R}$ is the constant upper bound. The observer after alarm is designed to be

$$\begin{aligned}
 \dot{\hat{X}} & = A\hat{X} + [f(\hat{X}) - A]\hat{X} + \phi(\hat{X}) + R[\tau(t - t_d) \\
 & \quad + \gamma(t - T)\tau_{\text{wave}} + \hat{\tau}_{\text{wind}}] + L[CX - C\hat{X}] \\
 & = f(\hat{X})\hat{X} + \phi(\hat{X}) + R[\tau(t - t_d) + \hat{W}_d^T S(\hat{Z}_{ow}) \\
 & \quad + \hat{\tau}_{\text{wind}}] + L[CX - C\hat{X}]
 \end{aligned} \tag{15}$$

where \hat{X} is the estimation of X . $L = P^{-1}C^T \in \mathbb{R}^{6 \times 6}$ is a observer gain matrix. $C \in \mathbb{R}^{6 \times 6}$ is the measurement matrix. $\hat{\tau}_{\text{wind}}$ denotes the wind force estimator to be developed later. Define the observer error as $\tilde{X} = X - \hat{X}$. The derivative of \tilde{X} is

$$\begin{aligned}
 \dot{\tilde{X}} & = \dot{X} - \dot{\hat{X}} \\
 & = (A - LC)\tilde{X} + [(f(X) - A)X + \phi(X) - (f(\hat{X}) \\
 & \quad - A)\hat{X} - \phi(\hat{X})] + R[\tau_{\text{wind}} - \hat{\tau}_{\text{wind}} + \tilde{W}_d^T S(\hat{Z}_{ow}) \\
 & \quad + \Lambda + d]
 \end{aligned} \tag{16}$$

For stability analysis of error signals, the following Lyapunov candidate is considered

$$V = \tilde{X}^T P \tilde{X} + \frac{1}{2} \tilde{\Phi}^T \Gamma^{-1} \tilde{\Phi} + \sum_{i=1}^6 \frac{1}{\omega_i} \tilde{W}_{di}^T \tilde{W}_{di} \tag{17}$$

where $\omega_i, (i = 1, 2, \dots, 6)$ is a constant value. The error of wind coefficient estimation $\tilde{\Phi}$ is

$$\tilde{\Phi} = \Phi - \hat{\Phi} \tag{18}$$

Incorporating (16), the time derivative of V gives

$$\begin{aligned}
 \dot{V} & = 2\tilde{X}^T P \dot{\tilde{X}} + \dot{\tilde{\Phi}}^T \Gamma^{-1} \tilde{\Phi} + \sum_{i=1}^n \frac{2}{\omega_i} \tilde{W}_{di}^T \dot{\tilde{W}}_{di} \\
 & = 2\tilde{X}^T P [(A - LC)\tilde{X} + [(f(X) - A)X + \phi(X) \\
 & \quad - (f(\hat{X}) - A)\hat{X} - \phi(\hat{X})] + R(\tau_{\text{wind}} - \hat{\tau}_{\text{wind}} + \tilde{W}_d^T \\
 & \quad S(\hat{Z}_{ow}) + \Lambda + d)] + \dot{\tilde{\Phi}}^T \Gamma^{-1} \tilde{\Phi} + \sum_{i=1}^n \frac{2}{\omega_i} \tilde{W}_{di}^T \dot{\tilde{W}}_{di}
 \end{aligned} \tag{19}$$

Consider Assumption 4, \dot{V} becomes

$$\begin{aligned}
 \dot{V} & \leq 2\tilde{X}^T P [(A - LC)\tilde{X} + R(\tau_{\text{wind}} - \hat{\tau}_{\text{wind}} + \tilde{W}_d^T \\
 & \quad S(\hat{Z}_{ow}) + \Lambda + d)] + 2\sigma \|P\tilde{X}\| \|\tilde{X}\| + \dot{\tilde{\Phi}}^T \Gamma^{-1} \tilde{\Phi}
 \end{aligned}$$

$$\begin{aligned}
 & + \sum_{i=1}^n \frac{2}{\omega_i} \tilde{W}_{di}^T \dot{\tilde{W}}_{di} \\
 & = 2\tilde{X}^T P(A - LC)\tilde{X} + 2\tilde{X}^T PR(\Pi\Phi - \hat{\tau}_{\text{wind}} \\
 & \quad + \tilde{W}_d^T S(\hat{Z}_{ow}) + \Lambda + d) + 2\sigma \|P\tilde{X}\| \|\tilde{X}\| \\
 & \quad + \dot{\tilde{\Phi}}^T \Gamma^{-1} \tilde{\Phi} + \sum_{i=1}^n \frac{2}{\omega_i} \tilde{W}_{di}^T \dot{\tilde{W}}_{di}
 \end{aligned} \tag{20}$$

The adaptive law of $\hat{\Phi}$ is designed as

$$\dot{\hat{\Phi}} = 2\Gamma^T \Pi^T R^T P^T \tilde{X} \tag{21}$$

With the adaptive law above, we have

$$\dot{\tilde{\Phi}}^T \Gamma^{-1} \tilde{\Phi} = -2\tilde{X}^T PR\Pi\tilde{\Phi} \tag{22}$$

Consequently, the wind force estimation term $\hat{\tau}_{\text{wind}}$ can be calculated as

$$\hat{\tau}_{\text{wind}} = \Pi\hat{\Phi} \tag{23}$$

Substituting (22) and (23) into (20), we obtain

$$\begin{aligned}
 \dot{V} & \leq 2\tilde{X}^T P(A - LC)\tilde{X} + 2\tilde{X}^T PR(\Pi\Phi - \Pi\hat{\Phi} + \tilde{W}_d^T \\
 & \quad S(\hat{Z}_{ow}) + \Lambda + d) + 2\sigma_d \|P\tilde{X}\| \|\tilde{X}\| - 2\tilde{X}^T PR\Pi\hat{\Phi} \\
 & \quad + \sum_{i=1}^n \frac{2}{\omega_i} \tilde{W}_{di}^T \dot{\tilde{W}}_{di} \\
 & = 2\tilde{X}^T P(A - LC)\tilde{X} + 2\tilde{X}^T PR(\tilde{W}_d^T S(\hat{Z}_{ow}) + \Lambda \\
 & \quad + d) + 2\sigma_d \|P\tilde{X}\| \|\tilde{X}\| + \sum_{i=1}^n \frac{2}{\omega_i} \tilde{W}_{di}^T \dot{\tilde{W}}_{di}
 \end{aligned} \tag{24}$$

Designing the adaptation for the weights in NN as

$$\dot{\tilde{W}}_{di} = -\omega_i (\tilde{X}^T PR)_i S(\hat{Z}_{ow}) \tag{25}$$

where $(\bullet)_i, (i = 1, 2, \dots, 6)$ is the i th column of \bullet . Invoking the update law into (24), we further have

$$\dot{V} \leq 2\tilde{X}^T P(A - LC)\tilde{X} + 2\tilde{X}^T PR(\Lambda + d) + 2\sigma_d \|P\tilde{X}\| \|\tilde{X}\| \tag{26}$$

Lemma 1: [22] For any two matrices X_{l1} and Y_{l1} of the same dimension, there exists a positive constant c_{l1} such that the following inequality holds.

$$X_{l1}^T Y_{l1} + Y_{l1}^T X_{l1} \leq c_{l1} X_{l1}^T X_{l1} + c_{l1}^{-1} Y_{l1}^T Y_{l1} \tag{27}$$

Since $2\tilde{X}^T PR(\Lambda + d)$ is a scalar and considering Lemma 1, Assumption 2 and (14), we have the following inequalities.

$$\begin{aligned}
 2\tilde{X}^T PR\Lambda & = \tilde{X}^T PR\Lambda + \Lambda^T R^T P^T \tilde{X} \leq \kappa_1 \tilde{X}^T PRR^T \\
 P^T \tilde{X} + \kappa_1^{-1} \Lambda^T \Lambda & \leq \kappa_1 \tilde{X}^T PRR^T P^T \tilde{X} + \kappa_1^{-1} \bar{\Lambda}
 \end{aligned} \tag{28}$$

$$\begin{aligned}
 2\tilde{X}^T PRd & = \tilde{X}^T PRd + d^T R^T P^T \tilde{X} \leq \kappa_2 \tilde{X}^T PRR^T \\
 P^T \tilde{X} + \kappa_2^{-1} d^T d & \leq \kappa_2 \tilde{X}^T PRR^T P^T \tilde{X} + \kappa_2^{-1} \bar{d}
 \end{aligned} \tag{29}$$

Moreover, it is clear that the following fact is held:

$$2\sigma_d \|P\tilde{X}\| \|\tilde{X}\| \leq 2\sigma_d \|\lambda_{\max}(P)\tilde{X}\| \|\tilde{X}\|$$

$$= 2\sigma_d \lambda_{\max}(P) \|\tilde{X}\|^2 = \tilde{X}^T 2\sigma_d \lambda_{\max}(P) I \tilde{X} \quad (30)$$

where $\lambda_{\max}(\bullet)$ is the maximum eigenvalue of \bullet . Substituting (28) (29) and (30) into (26) yields

$$\dot{V} \leq \tilde{X}^T (2PA - 2PLC + 2\sigma_d \lambda_{\max}(P)I + \kappa_1 PRR^T P^T + \kappa_2 PRR^T P^T) \tilde{X} + \kappa_1^{-1} \bar{\Lambda} + \kappa_2^{-1} \bar{d} \quad (31)$$

In accordance with $L = P^{-1}C^T$ and KYP lemma, (31) gives

$$\begin{aligned} \dot{V} &\leq \tilde{X}^T (A^T P + PA - 2C^T C + 2\sigma_d \lambda_{\max}(P)I + \kappa_1 PR \\ &\quad R^T P^T + \kappa_2 PRR^T P^T) \tilde{X} + \kappa_1^{-1} \bar{\Lambda} + \kappa_2^{-1} \bar{d} \\ &= \tilde{X}^T (-QQ^T - 2C^T C + 2\sigma_d \lambda_{\max}(P)I + \kappa_1 PRR^T P^T \\ &\quad + \kappa_2 PRR^T P^T) \tilde{X} + \kappa_1^{-1} \bar{\Lambda} + \kappa_2^{-1} \bar{d} \\ &= \tilde{X}^T E \tilde{X} + \kappa_1^{-1} \bar{\Lambda} + \kappa_2^{-1} \bar{d} \end{aligned} \quad (32)$$

where $E = -QQ^T - 2C^T C + 2\sigma_d \lambda_{\max}(P)I + (\kappa_1 + \kappa_2)PRR^T P^T$. By properly choosing A , P , Q , σ_d , κ_1 and κ_2 , E can be guaranteed to be negative definite and $\tilde{X}^T E \tilde{X} < 0$. If

$$-\tilde{X}^T E \tilde{X} = \tilde{X}^T (-E) \tilde{X} \geq \lambda_{\min}(-E) \|\tilde{X}\|^2 > \kappa_1^{-1} \bar{\Lambda} + \kappa_2^{-1} \bar{d} \quad (33)$$

we can ensure $\dot{V} < 0$. The stability condition above can be further expressed as

$$\|\tilde{X}\| > \sqrt{\frac{\kappa_1^{-1} \bar{\Lambda} + \kappa_2^{-1} \bar{d}}{\lambda_{\min}(-E)}} \quad (34)$$

Remark 2: By proper selection of the observer coefficients, the estimation error, i.e. \tilde{X} can be arbitrarily small.

Since only wind-induced forces and moment affecting the motion of the vessel before the vessel is subject to large wave-induced force, the wave force term $\gamma(t-T)\tau_{\text{wave}}$ in (9) can be ignored. The sea observer under this stage is proposed in the following pattern.

$$\dot{\hat{X}} = f(\hat{X})\hat{X} + \phi(\hat{X}) + R[\tau(t-t_d) + \Pi\hat{\Phi}] + L[CX - C\hat{X}] \quad (35)$$

Remark 3: The stability verification is very similar to the observer with NN estimator above thus is neglected. In practical use, when the sea state changes, the wind force estimator will overly compensate due to the involvement of the wave force. Therefore, we can judge the moment of alarm by monitoring the estimated wind drag coefficients. The NN compensator in both observer and controller are to be activated when a designed threshold for estimated wind drag coefficients are exceeded. The observer error \tilde{X} can also be applied as an axillary indicator for the alarm.

Remark 4: Based on the *Helmholtz-Kirchhoff* plate theory [16], the peak of wind drag coefficient is parameterized in terms of four shape-related parameters. Hence, for fixed vessel, the alarm threshold is unique and can be calculated approximately or through field calibration.

IV. ROBUST CONTROL DESIGN

In this section, we focus on an input time delay control with constrained tracking error. One approach to cope with the input time delay is to convert the original system into a delay-free system known as the Artstein model [23]. Essentially, Artstein model is a predictor-like controller for linear system. However, the dynamics of the vessel is of great nonlinearity and this model does not consider the limitation of tracking error. Therefore, inspired by [23] and combining BLF method [24], a model-based robust controller with input time delay and tracking error constraint is developed in this paper.

A. Design of control before alarm

The wind force is estimated using $\hat{\tau}_{\text{wind}}$ in the last section. Define the estimation error as $\tilde{\tau}_{\text{wind}} = \tau_{\text{wind}} - \hat{\tau}_{\text{wind}}$. When no large wave-induced drift force is detected, we consider the following dynamic system.

$$M\dot{\nu} + C(\nu)\nu + D(\nu)\nu + g(\eta) = \tau'(t-t_d) + d_1 \quad (36)$$

where $\tau'(t-t_d) = \tau(t-t_d) + \hat{\tau}_{\text{wind}}$, $d_1 = \tilde{\tau}_{\text{wind}} + d$ which performs as a feedforward control to cope with the wind force. While, the actuator delay of the feedforward control component $\hat{\tau}_{\text{wind}}$ is neglected in this work. The input delay t_d is assumed as a known constant value.

Remark 5: The estimation error of the peak of wind drag coefficient $\tilde{\Phi}$ has been proven to be bounded in the last section. Hence, the wind force estimation error $\tilde{\tau}_{\text{wind}}$ is bounded. Combining Assumption 2, the newly defined term d_1 is bounded and can be rationally limited as \bar{d}_1 with $\|d_1\| \leq \bar{d}_1$. Where \bar{d}_1 is a positive constant.

Incorporating Symmetry Barrier Lyapunov Function (SBLF) [24], a backstepping approach is employed to design the control.

Step 1: Denote

$$z_1 = \eta_d - \eta, \quad z_2 = \alpha_c - \nu \quad (37)$$

where the desired trajectory satisfies $\eta_d, \dot{\eta}_d \in \mathcal{L}_\infty$. α_c is the stabilizing function. Choose a positive definite and C^1 continuous SBLF candidate as

$$\begin{aligned} V_1 &= \frac{1}{2} \log \frac{N_b^T I_x N_b}{N_b^T I_x N_b - z_1^T I_x z_1} + \frac{1}{2} \log \frac{N_b^T I_y N_b}{N_b^T I_y N_b - z_1^T I_y z_1} \\ &\quad + \frac{1}{2} \log \frac{N_b^T I_\psi N_b}{N_b^T I_\psi N_b - z_1^T I_\psi z_1} \end{aligned} \quad (38)$$

where

$$I_x = \begin{bmatrix} 1 & 0 & 0 \\ 0 & 0 & 0 \\ 0 & 0 & 0 \end{bmatrix} \quad I_y = \begin{bmatrix} 0 & 0 & 0 \\ 0 & 1 & 0 \\ 0 & 0 & 0 \end{bmatrix} \quad I_\psi = \begin{bmatrix} 0 & 0 & 0 \\ 0 & 1 & 0 \\ 0 & 0 & 0 \end{bmatrix} \quad (39)$$

$N_b \in \mathbb{R}^{3 \times 1}$ is the tracking error constraint such that $|z_1| \leq N_b$ should be satisfied.

Remark 6: In practical use, the initial condition of position and velocity of the vessel are consistent with the desired trajectory. Hence, $|z_1(0)| < N_b$ can be guaranteed.

Time derivative of V_1 yields

$$\dot{V}_1 = \frac{z_1^T I_x \dot{z}_1}{N_b^T I_x N_b - z_1^T I_x z_1} + \frac{z_1^T I_y \dot{z}_1}{N_b^T I_y N_b - z_1^T I_y z_1}$$

$$+ \frac{z_1^T I_\psi \dot{z}_1}{N_b^T I_\psi N_b - z_1^T I_\psi z_1} \quad (40)$$

Differentiating z_1 with respect to time gives

$$\dot{z}_1 = \dot{\eta}_d - J(\eta_\psi)(\alpha_c - z_2) \quad (41)$$

Substituting (41) into (40), we have

$$\begin{aligned} \dot{V}_1 = & \frac{z_1^T I_x [\dot{\eta}_d - J(\eta_\psi)(\alpha_c - z_2)]}{N_b^T I_x N_b - z_1^T I_x z_1} + \frac{z_1^T I_y [\dot{\eta}_d - J(\eta_\psi)(\alpha_c - z_2)]}{N_b^T I_y N_b} \\ & \frac{(\alpha_c - z_2)}{-z_1^T I_y z_1} + \frac{z_1^T I_\psi [\dot{\eta}_d - J(\eta_\psi)(\alpha_c - z_2)]}{N_b^T I_\psi N_b - z_1^T I_\psi z_1} \end{aligned} \quad (42)$$

Design the stabling function α_c to be

$$\alpha_c = J^T(\eta_\psi)[\dot{\eta}_d + (N_b^T N_b - z_1^T z_1)K_1 z_1] \quad (43)$$

Substituting (43) into (42) and considering the property of rotation matrix $J(\eta_\psi)J^T(\eta_\psi) = I$, following equation is achieved.

$$\begin{aligned} \dot{V}_1 = & -3z_1^T K_1 z_1 + \frac{z_1^T I_x J(\eta_\psi) z_2}{N_b^T I_x N_b - z_1^T I_x z_1} \\ & + \frac{z_1^T I_y J(\eta_\psi) z_2}{N_b^T I_y N_b - z_1^T I_y z_1} + \frac{z_1^T I_\psi J(\eta_\psi) z_2}{N_b^T I_\psi N_b - z_1^T I_\psi z_1} \end{aligned} \quad (44)$$

Step 2: Define an auxiliary state $S \in \mathbb{R}^{3 \times 1}$ to compensate for the input delay with the following expression.

$$S = z_2 - M^{-1} \int_{t-t_d}^t \tau'(\theta) d\theta - z_f \quad (45)$$

where $z_f \in \mathbb{R}^{3 \times 1}$ satisfies the following adaptive law.

$$\dot{z}_f = K_2 S - \Gamma_1 z_2 - \Theta z_f \quad (46)$$

In (46), $K_2, \Gamma_1, \Theta \in \mathbb{R}^{3 \times 3}$ are positive tuning parameters. Multiply both sides of (45) by M and denote $M_s = C(\nu) + D(\nu) + g(\eta)$, the derivative of MS yields

$$\begin{aligned} M\dot{S} = & M\dot{z}_2 - \tau'(t) + \tau'(t-t_d) - \dot{z}_f \\ = & M\dot{\alpha}_c + C(\nu)\nu + D(\nu)\nu + g(\eta) - d_1 - \tau'(t) \\ & - K_2 S + \Theta z_f + \Gamma_1 z_2 \\ = & M\dot{\alpha}_c + M_s - d_1 + N_c - \tau'(t) - K_2 S - K_2 z_2 \\ & - (S^T)^+ \dot{S}^T z_2 \end{aligned} \quad (47)$$

where N_c is defined as follows and consider the Mean Value Theorem [25].

$$\begin{aligned} N_c = & \Theta z_f + \Gamma_1 z_2 + K_2 z_2 + (S^T)^+ \dot{S}^T z_2 \\ ||N_c|| \leq & \overline{N}_c(||z_s||) ||z_s|| \end{aligned} \quad (48)$$

where the bounding function $\overline{N}_c(||z_s||)$ is a globally positive function. z_s has the definition of $z_s = [z_1^T, z_2^T, S^T, z_\tau^T, z_f^T]^T$, where $z_\tau \in \mathbb{R}^{3 \times 1}$ denotes

$$z_\tau = \tau'(t) - \tau'(t-\beta) = \int_{t-t_d}^t \dot{\tau}'(\theta) d\theta \quad (49)$$

With the involvement of auxiliary state S , the delayed system is converted into a delay-free one as shown in (47). For the velocity of the vessel, no limitation is needed. Thus, a quadratic form Lyapunov-Krasovskii candidate function is

defined as [26]

$$\begin{aligned} V_2 = & V_1 + \frac{1}{2} z_2^T z_2 + \frac{1}{2} S^T M S + \frac{1}{2} z_f^T z_f \\ & + v \int_{t-t_d}^t \left(\int_w^t ||\dot{\tau}'(\theta)||^2 d\theta \right) dw \end{aligned} \quad (50)$$

Differentiating V_2 and invoking (44), (45), (46) and (47), we obtain

$$\begin{aligned} \dot{V}_2 = & \dot{V}_1 + z_2^T \dot{z}_2 + S^T M \dot{S} + z_f^T \dot{z}_f + vt_d ||\dot{\tau}'(\theta)||^2 \\ & - v \int_{t-t_d}^t ||\dot{\tau}'(\theta)||^2 d\theta \\ = & -3z_1^T K_1 z_1 + \frac{z_1^T I_x J(\eta_\psi) z_2}{N_b^T I_x N_b - z_1^T I_x z_1} \\ & + \frac{z_1^T I_y J(\eta_\psi) z_2}{N_b^T I_y N_b - z_1^T I_y z_1} + \frac{z_1^T I_\psi J(\eta_\psi) z_2}{N_b^T I_\psi N_b - z_1^T I_\psi z_1} \\ & + z_2^T (\dot{S} - M^{-1}(\tau(t-t_d) - \tau(t)) + K_2 S - \Theta z_f \\ & - \Gamma_1 z_2) + S^T (M\dot{\alpha}_c + M_s - d_1 + N_c - \tau(t)' \\ & - K_2 S - K_2 z_2 - (S^T)^+ \dot{S}^T z_2) + z_f^T K_2 S - z_f^T \Theta z_f \\ & - z_f^T \Gamma_1 z_2 + vt_d ||\dot{\tau}'(\theta)||^2 - v \int_{t-t_d}^t ||\dot{\tau}'(\theta)||^2 d\theta \\ = & -3z_1^T K_1 z_1 + \frac{z_1^T I_x J(\eta_\psi) z_2}{N_b^T I_x N_b - z_1^T I_x z_1} \\ & + \frac{z_1^T I_y J(\eta_\psi) z_2}{N_b^T I_y N_b - z_1^T I_y z_1} + \frac{z_1^T I_\psi J(\eta_\psi) z_2}{N_b^T I_\psi N_b - z_1^T I_\psi z_1} \\ & - z_2^T \Gamma_1 z_2 + z_2^T M^{-1} z_\tau - z_2^T (\Gamma_1 + I) z_f - S^T K_2 S \\ & + S^T [M\dot{\alpha}_c + M_s - d_1 + N_c - \tau'(t)] + z_f^T K_2 S \\ & - z_f^T \Theta z_f + vt_d ||\dot{\tau}'(\theta)||^2 - v \int_{t-t_d}^t ||\dot{\tau}'(\theta)||^2 d\theta \end{aligned} \quad (51)$$

Design the following control law

$$\begin{aligned} \tau'(t) = & M\dot{\alpha}_c + M_s + K_2 z_f + (S^T)^+ \left[\frac{z_1^T I_x J(\eta_\psi) z_2}{N_b^T I_x N_b - z_1^T I_x z_1} \right. \\ & + \frac{z_1^T I_y J(\eta_\psi) z_2}{N_b^T I_y N_b - z_1^T I_y z_1} + \frac{z_1^T I_\psi J(\eta_\psi) z_2}{N_b^T I_\psi N_b - z_1^T I_\psi z_1} \\ & + \frac{N_b^T I_x N_b z_1^T K_1 z_1}{N_b^T I_x N_b - z_1^T I_x z_1} + \frac{N_b^T I_y N_b z_1^T K_1 z_1}{N_b^T I_y N_b - z_1^T I_y z_1} \\ & \left. + \frac{N_b^T I_\psi N_b z_1^T K_1 z_1}{N_b^T I_\psi N_b - z_1^T I_\psi z_1} \right] \end{aligned} \quad (52)$$

Substitute (52) into (51) and considering (48) and Assumption 1, we have

$$\begin{aligned} \dot{V}_2 = & -3z_1^T K_1 z_1 - z_2^T \Gamma_1 z_2 - S^T K_2 S - z_f^T \Theta z_f + z_2^T M^{-1} \\ & z_\tau - z_2^T (\Gamma_1 + I) z_f + S^T N_c - S^T d_1 + vt_d ||\dot{\tau}'(\theta)||^2 \\ & - v \int_{t-t_d}^t ||\dot{\tau}'(\theta)||^2 d\theta - \frac{N_b^T I_x N_b z_1^T K_1 z_1}{N_b^T I_x N_b - z_1^T I_x z_1} \\ & - \frac{N_b^T I_y N_b z_1^T K_1 z_1}{N_b^T I_y N_b - z_1^T I_y z_1} - \frac{N_b^T I_\psi N_b z_1^T K_1 z_1}{N_b^T I_\psi N_b - z_1^T I_\psi z_1} \\ \leq & -3z_1^T K_1 z_1 - \lambda_{\min}(\Gamma_1) z_2^T z_2 - S^T K_2 S \\ & - \lambda_{\min}(\Theta) z_f^T z_f + \overline{M}^{-1} ||z_2|| ||z_\tau|| + (-\Gamma_1 - I) \\ & ||z_2|| ||z_f|| + \overline{N}_c(||z_s||) ||z_s|| ||S|| + \overline{d}_1 ||S|| + vt_d \end{aligned}$$

$$\begin{aligned} & \|\dot{\tau}'(\theta)\|^2 - v \int_{t-t_d}^t \|\dot{\tau}'(\theta)\|^2 d\theta - \frac{N_b^T I_x N_b z_1^T K_1 z_1}{N_b^T I_x N_b - z_1^T I_x z_1} \\ & - \frac{N_b^T I_y N_b z_1^T K_1 z_1}{N_b^T I_y N_b - z_1^T I_y z_1} - \frac{N_b^T I_\psi N_b z_1^T K_1 z_1}{N_b^T I_\psi N_b - z_1^T I_\psi z_1} \end{aligned} \quad (53)$$

To facilitate the subsequent analysis, the Young's inequality is introduced.

$$\|a\| \|b\| \leq \frac{\iota}{4} \|a\|^2 + \frac{1}{\iota} \|b\|^2 \quad (54)$$

where a and b are vectors, ι is a positive constant. Therefore, the $\overline{N}_c(\|z_s\|)\|z_s\|\|S\|$ term in (53) yields

$$\begin{aligned} \overline{N}_c(\|z_s\|)\|z_s\|\|S\| & \leq \frac{\sigma_3 \overline{N}_c^2(\|z_s\|)\|z_s\|^2}{4} + \frac{1}{\sigma_3} \|S\|^2 \\ & \leq \frac{\sigma_3 \overline{N}_c^2(\|z_s\|)(\|z_1\|^2 + \|z_2\|^2 + \|S\|^2 + \|z_\tau\|^2}{4} \\ & + \|z_f\|^2 + \frac{1}{\sigma_3} \|S\|^2 \end{aligned} \quad (55)$$

Similar situation holds for other terms in (53). Moreover, under the condition of $\|z_1\| < \|N_b\|$, the following inequalities holds.

$$\begin{aligned} & \frac{\sigma_3 \overline{N}_c^2(\|z_s\|) z_1^T z_1 - z_1^T K_1 z_1}{12 \overline{N}_c^2(\|z_s\|) z_1^T z_1 - z_1^T K_1 z_1} - \frac{N_b^T I_x N_b z_1^T K_1 z_1}{N_b^T I_x N_b - z_1^T I_x z_1} \\ & \leq - \frac{(\lambda_{\min}(K_1) - \frac{\sigma_3 \overline{N}_c^2(\|z_s\|)}{12}) N_b^T I_x N_b z_1^T I_x z_1}{N_b^T I_x N_b - z_1^T I_x z_1} \\ & \leq - \left(\lambda_{\min}(K_1) - \frac{\sigma_3 \overline{N}_c^2(\|z_s\|)}{12} \right) N_b^T I_x N_b \\ & \log \frac{N_b^T I_x N_b}{N_b^T I_x N_b - z_1^T I_x z_1} \end{aligned} \quad (56)$$

For y and ψ , we have identical transformation. Herein, define

$$\begin{aligned} \Xi_x & = - \left(\lambda_{\min}(K_1) - \frac{\sigma_3 \overline{N}_c^2(\|z_s\|)}{12} \right) N_b^T I_x N_b \\ & \log \frac{N_b^T I_x N_b}{N_b^T I_x N_b - z_1^T I_x z_1} \\ \Xi_y & = - \left(\lambda_{\min}(K_1) - \frac{\sigma_3 \overline{N}_c^2(\|z_s\|)}{12} \right) N_b^T I_y N_b \\ & \log \frac{N_b^T I_y N_b}{N_b^T I_y N_b - z_1^T I_y z_1} \\ \Xi_\psi & = - \left(\lambda_{\min}(K_1) - \frac{\sigma_3 \overline{N}_c^2(\|z_s\|)}{12} \right) N_b^T I_\psi N_b \\ & \log \frac{N_b^T I_\psi N_b}{N_b^T I_\psi N_b - z_1^T I_\psi z_1} \end{aligned} \quad (57)$$

Combining (54),(55), (56) and (57), (53) can be revised as

$$\begin{aligned} \dot{V}_2 & \leq \Xi_x + \Xi_y + \Xi_\psi - [\lambda_{\min}(\Gamma_1) - \frac{\sigma_3 \overline{N}_c^2(\|z_s\|)}{4}] z_2^T z_2 \\ & - [\lambda_{\min}(K_2) - \frac{\sigma_3 \overline{N}_c^2(\|z_s\|)}{4}] S^T S - [\lambda_{\min}(\Theta_1) \\ & - \frac{\sigma_3 \overline{N}_c^2(\|z_s\|)}{4}] z_f^T z_f + \frac{\sigma_1 \overline{M}^{-1}}{4} \|z_2\|^2 \\ & + \left[\frac{1}{\sigma_1} + \frac{\sigma_3 \overline{N}_c^2(\|z_s\|)}{4} \right] \|z_\tau\|^2 + \frac{\sigma_2 \overline{(-\Gamma_1 - I)}^2}{4} \\ & \|z_2\|^2 + \frac{1}{\sigma_2} \|z_f\|^2 + \frac{1}{\sigma_3} \|S\|^2 + \frac{\sigma_4 \overline{d}_1^2}{4} + \frac{1}{\sigma_4} \|S\|^2 \end{aligned}$$

$$+ v t_d \|\dot{\tau}'(\theta)\|^2 - v \int_{t-t_d}^t \|\dot{\tau}'(\theta)\|^2 d\theta \quad (58)$$

Cauchy-Schwarz inequality gives the upper bound of $\|z_\tau\|$ as

$$\|z_\tau\|^2 \leq t_d \int_{t-t_d}^t \|\dot{\tau}'(\theta)\|^2 d\theta \quad (59)$$

Moreover, it can be proven that

$$\int_{t-t_d}^t \left[\int_w^t \|\dot{\tau}'(\theta)\|^2 d\theta \right] dw \leq t_d \int_{t-t_d}^t \|\dot{\tau}'(\theta)\|^2 d\theta \quad (60)$$

With (59) and (60), (58) becomes

$$\begin{aligned} \dot{V}_2 & \leq \Xi_x + \Xi_y + \Xi_\psi - \left[\lambda_{\min}(\Gamma_1) - \frac{\sigma_1 \overline{M}^{-1}}{4} - \frac{\sigma_3 \overline{N}_c^2(\|z_s\|)}{4} \right. \\ & - \frac{\sigma_2 \overline{(-\Gamma_1 - I)}^2}{4} \left. \right] z_2^T z_2 - \left[\lambda_{\min}(K_2) - \frac{1}{\sigma_3} - \frac{1}{\sigma_4} - \frac{\sigma_3}{4} \right. \\ & \overline{N}_c^2(\|z_s\|) \left. \right] S^T S - \left[\lambda_{\min}(\Theta_1) - \frac{1}{\sigma_2} - \frac{\sigma_3 \overline{N}_c^2(\|z_s\|)}{4} \right] \\ & z_f^T z_f + \frac{\sigma_4 \overline{d}_1^2}{4} + v t_d \|\dot{\tau}'(\theta)\|^2 - \left[v - \frac{t_d}{\sigma_1} \right. \\ & - \left. \frac{t_d \sigma_3 \overline{N}_c^2(\|z_s\|)}{4} \right] \int_{t-t_d}^t \|\dot{\tau}'(\theta)\|^2 d\theta \\ & \leq \Xi_x + \Xi_y + \Xi_\psi - \left[\lambda_{\min}(\Gamma_1) - \frac{\sigma_1 \overline{M}^{-1}}{4} - \frac{\sigma_3 \overline{N}_c^2(\|z_s\|)}{4} \right. \\ & - \frac{\sigma_2 \overline{(-\Gamma_1 - I)}^2}{4} \left. \right] z_2^T z_2 - \left[\lambda_{\min}(K_2) - \frac{1}{\sigma_3} - \frac{1}{\sigma_4} \right. \\ & - \left. \frac{\sigma_3 \overline{N}_c^2(\|z_s\|)}{4} \right] S^T S - \left[\lambda_{\min}(\Theta_1) - \frac{1}{\sigma_2} \right. \\ & - \left. \frac{\sigma_3 \overline{N}_c^2(\|z_s\|)}{4} \right] z_f^T z_f - \left[\frac{v}{t_d} - \frac{1}{\sigma_1} - \frac{\sigma_3 \overline{N}_c^2(\|z_s\|)}{4} \right] \\ & \int_{t-t_d}^t \left[\int_w^t \|\dot{\tau}'(\theta)\|^2 d\theta \right] dw + \frac{\sigma_4 \overline{d}_1^2}{4} + v t_d \|\dot{\tau}'(\theta)\|^2 \\ & \leq -\rho_c V_2 + \beta_c \end{aligned} \quad (61)$$

where $\rho_c, \beta_c > 0$ and they satisfy $\rho_c =$

$$\begin{aligned} & \min \left[2\Xi_x, 2\Xi_y, 2\Xi_{\psi}, 2(\lambda_{\min}(\Gamma_1) - \frac{\sigma_1 \overline{M}^{-1}}{4} - \frac{\sigma_3 \overline{N}_c^2(\|z_s\|)}{4} - \frac{\sigma_2 \overline{(-\Gamma_1 - I)}^2}{4}), 2(\lambda_{\min}(K_2) - \frac{1}{\sigma_3} - \frac{1}{\sigma_4} - \frac{\sigma_3 \overline{N}_c^2(\|z_s\|)}{4}) / \lambda_{\max}(M), 2(\lambda_{\min}(\Theta_1) - \frac{1}{\sigma_2} - \frac{\sigma_3 \overline{N}_c^2(\|z_s\|)}{4}), \left(\frac{1}{t_d} - \frac{1}{\sigma_1} - \frac{\sigma_3 \overline{N}_c^2(\|z_s\|)}{4} \right) \right] \text{ with the} \\ & \text{tuning parameters are selected } \lambda_{\min}(K_1) > \frac{\sigma_3 \overline{N}_c^2(\|z_s\|)}{12}, \\ & \lambda_{\min}(\Gamma_1) + \frac{\sigma_2 \overline{(-\Gamma_1 - I)}^2}{4} > \frac{\sigma_1 \overline{M}^{-1}}{4} + \frac{\sigma_3 \overline{N}_c^2(\|z_s\|)}{4}, \\ & \lambda_{\min}(K_2) > \frac{1}{\sigma_3} + \frac{1}{\sigma_4} + \frac{\sigma_3 \overline{N}_c^2(\|z_s\|)}{4}, \lambda_{\min}(\Theta_1) > \\ & \frac{1}{\sigma_2} + \frac{\sigma_3 \overline{N}_c^2(\|z_s\|)}{4}, \frac{v}{t_d} > \frac{1}{\sigma_1} + \frac{\sigma_3 \overline{N}_c^2(\|z_s\|)}{4}. \\ & \beta_c = \frac{\sigma_4 \overline{d}_1^2}{4} + v t_d \|\dot{\tau}'(\theta)\|^2. \end{aligned}$$

Lemma 2: [27] [28] For bounded initial conditions, if there exists a C^1 continuous and positive definite Lyapunov function

$V(x)$ satisfying $v_1(\|x\|) \leq V(x) \leq v_2(\|x\|)$, such that $\dot{V} \leq -\alpha V(x) + \beta$, where $v_1, v_2: \mathbb{R}^n \rightarrow \mathbb{R}$ are class K functions and $\alpha, \beta > 0$, then the solution $x(t)$ is uniformly bounded.

Remark 7: Combining Lemma 2, Remark 6 and (37)-(61), the Semi-Globally Uniform Boundness (SGUB) of all the signals are guaranteed under the existence of input delay. In addition, the tracking error is regulated as $|z_1| \leq N_b$.

B. Design of control after alarm

For robust control under large wave-induced force, we consider the model in (1) (2). Similar to the control before alarm, the wind force is estimated for the feedforward control. Thus, the dynamic model of (2) can be rewritten as

$$M\dot{\nu} + C(\nu)\nu + D(\nu)\nu + g(\eta) = \tau'(t-t_d) + \gamma(t-T)\tau_{\text{wave}} + d_1 \quad (62)$$

For simplicity, in the following proof, the term $\gamma(t-T)\tau_{\text{wave}}$ will be replaced by τ_{wave} . The first step of the control design after alarm is the same with *step 1*. And all the proof before (46) remain the same, (47) will be changed into

$$M\dot{S} = M\dot{\alpha}_c + M_s - \tau_{\text{wave}} - d_1 + N_c - \tau'(t) - K_2S - K_2z_2 - (S^T)^+ \hat{S}^T z_2 \quad (63)$$

To estimate the unknown wave force, a RBF neural network is applied.

$$\tau_{\text{wave}} = W_c^{*T} S_c(Z_c) + \epsilon_c \quad (64)$$

Denote $\hat{W}_c, W_c^*, \epsilon_c$ as the estimated weights, optimal weights and approximation error respectively. Z_c is the input vector to the neural network. The details about Z_c will be introduced in the simulation section. Design the update law of the NN weights to be

$$\dot{\hat{W}}_{ci} = -\Upsilon_i(S_{ci}(Z_c)S_i + \xi_i\hat{W}_{ci}) \quad (65)$$

Control input under this condition should be augmented into

$$\tau'_m(t) = \tau'(t) - \hat{W}_c^T S_c(Z_c) \quad (66)$$

The control law in (66) is able to guarantee the SGUB of all the close-loop system states.

Proof The proof is very trivial and similar to that in ‘‘control before alarm’’ section, thus, ignore here.

V. OPTIMAL THRUST ALLOCATION FOR DYNAMIC POSITIONING

A. Problem Formulation for Thrust Allocation

This section will give an optimal solution in terms of individual thruster to achieve required resultant force along axis X and Y and resultant torque M_z . The AV DP system is compounded by 6 nozzle thrusters. Each of them can rotate the full 360° to generate thrust in any direction. The six thrusters are grouped in pairs and their layout are presented in Fig. 3.

In addition, to avoid thruster-thruster interaction, a forbidden zone [29] of 20° is considered to increase the propelling efficiency. The forbidden zone in this paper is depicted as Fig. 4.

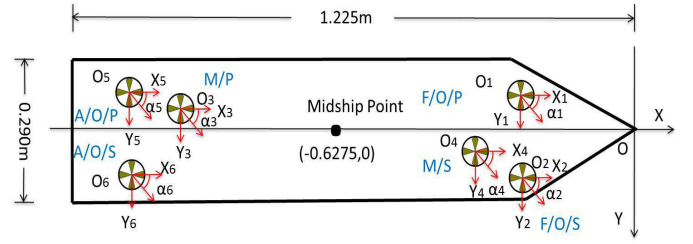


Fig. 3. Thruster layout and coordinate system

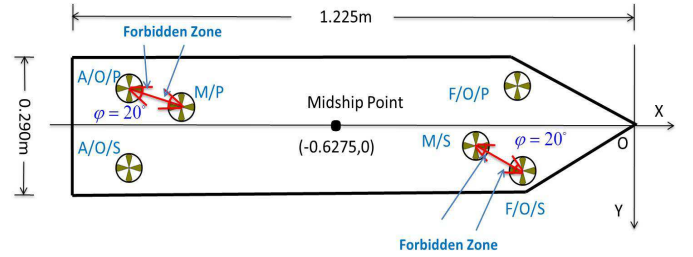


Fig. 4. Definition of The Forbidden Zone

The resulting force and moment generated by the 6 thrusters in surge, sway and yaw direction are given by

$$F_x = \sum_{i=1}^6 \cos \alpha_i u_i = A_{f_x}(\alpha)u, F_y = \sum_{i=1}^6 \sin \alpha_i u_i = A_{f_y}(\alpha)u \quad (67)$$

$$M_z = (l_{1x} \cos \alpha_1 + l_{1y} \sin \alpha_1)u_1 + (-l_{2x} \cos \alpha_2 + l_{2y} \sin \alpha_2)u_2 + (l_{3x} \cos \alpha_3 - l_{3y} \sin \alpha_3)u_3 + (-l_{4x} \cos \alpha_4 + l_{4y} \sin \alpha_4)u_4 + (l_{5x} \cos \alpha_5 - l_{5y} \sin \alpha_5)u_5 + (-l_{6x} \cos \alpha_6 - l_{6y} \sin \alpha_6)u_6 = A_M(\alpha)u \quad (68)$$

where l_{ix} and l_{iy} ($i=1,2,\dots,6$) are the moment arm along X and Y direction of the i th thruster. α_i and u_i are the rotation angle and the magnitude of thrust produced by the i th thruster. α_i s and u_i s are merged as $\alpha = [\alpha_1, \alpha_2, \alpha_3, \alpha_4, \alpha_5, \alpha_6]^T$ and $u = [u_1, u_2, u_3, u_4, u_5, u_6]^T$. The sum of generalized propelling forces on the vessel from the thrusters are modelled as

$$\tau = \mathcal{T}(\alpha)u \quad (69)$$

where $\mathcal{T}(\alpha) = [A_{f_x}(\alpha), A_{f_y}(\alpha), A_M(\alpha)]^T$. τ is the command signal which is the combination of feedforward wind force compensation and the feedback control effort designed in the last section. The cost function is formulated as

$$J = \min\{u^T Q u + (\alpha - \alpha_0)^T \mathcal{P}(\alpha - \alpha_0) + o^T \mathcal{R} o\} \quad (70)$$

subject to:

$$\mathcal{T}(\alpha)u = \tau + o, \quad \underline{u} \leq u \leq \bar{u}, \quad \underline{\alpha} \leq \alpha \leq \bar{\alpha} \quad (71)$$

$$\underline{\Delta\alpha} \leq \alpha - \alpha_0 \leq \overline{\Delta\alpha} \quad (72)$$

where $u^T Q u$ represents power consumption and $Q \in \mathbb{R}^{6 \times 6}$ is a positive weight matrix. The second term of the cost function

is used to guarantee a minimum rotation angle of each thruster in a single sampling interval with positive weights $\mathcal{P} \in \mathbb{R}^{6 \times 6}$. $\alpha_0 \in \mathbb{R}^{6 \times 1}$ represent current rotated angle of the thrusters. $o^T \mathcal{R} o$ penalizes the error $o \in \mathbb{R}^{3 \times 1}$ between the commanded and achieved generalized force. The weight $\mathcal{R} \in \mathbb{R}^{3 \times 3}$ should be chosen sufficiently large so that the error is necessarily small. $\underline{u} \leq u \leq \bar{u}$ denotes the limit of thrust in this case. $\underline{\alpha} \leq \alpha \leq \bar{\alpha}$ restricts the feasible working zone, in this case, 20° forbidden zone is considered. $\underline{\Delta\alpha} \leq \alpha - \alpha_0 \leq \bar{\Delta\alpha}$ gives the constrain of azimuth speed.

B. Locally Convex Reformulation

The above formulation usually contributes to a nonlinear non-convex problem which requires large computations to search the solution. The main reason is the nonlinearity of the equality constraint (71). To simplify the solution search process, a locally convex quadratic programming reformulation is suggested. Since in dynamic positioning the azimuth angles are required to be slowly varying near the position in last sampling time instant α_0 and similar situation holds for the output thrust, linearization of the equality constraint at the current thruster state (output thrust and angle) is reasonable. Therefore, the optimization problem can be reformulated as follows.

$$\begin{aligned} J &= \min\{(u_0 + \Delta u)^T \mathcal{Q}(u_0 + \Delta u) + \Delta\alpha^T \mathcal{P} \Delta\alpha + o^T \mathcal{R} o\} \\ &= \min\{\Delta u^T \mathcal{Q} \Delta u + \Delta\alpha^T \mathcal{P} \Delta\alpha + o^T \mathcal{R} o + (2\mathcal{Q}^T u_0)^T \Delta u\} \end{aligned} \quad (73)$$

subject to:

$$\mathcal{T}(\alpha_0) \Delta u + \left. \frac{\partial}{\partial \alpha} (\mathcal{T}(\alpha) u) \right|_{\alpha_0, u_0} \Delta\alpha - o = \tau - \mathcal{T}(\alpha_0) u_0 \quad (74)$$

$$\underline{u} - u_0 \leq \Delta u \leq \bar{u} - u_0, \quad \underline{\alpha} - \alpha_0 \leq \Delta\alpha \leq \bar{\alpha} - \alpha_0 \quad (75)$$

$$\underline{\Delta\alpha} \leq \Delta\alpha \leq \bar{\Delta\alpha} \quad (76)$$

The optimization problem above can be rewritten as the following more compact form.

$$J = \min\left\{\frac{1}{2} \mathcal{U}^T \mathcal{K} \mathcal{U} + \mathcal{W}^T \mathcal{U}\right\} \quad (77)$$

s.t.

$$\mathcal{M} \mathcal{U} = \mathcal{Y}, \quad \underline{\mathcal{U}} \leq \mathcal{U} \leq \bar{\mathcal{U}} \quad (78)$$

where $\mathcal{U} = [\Delta u^T, \Delta\alpha^T, o^T]^T \in \Omega_{\mathcal{U}}$, $\Omega_{\mathcal{U}} := \{\mathcal{U} \in \mathbb{R}^{6 \times 1} | \underline{\mathcal{U}} \leq \mathcal{U} \leq \bar{\mathcal{U}}\}$. Other vectors and matrices are defined as $\mathcal{K} = \text{diag}[2\mathcal{Q}, 2\mathcal{P}, 2\mathcal{R}]$, $\mathcal{W} = [(2\mathcal{Q}^T u_0)^T, O_{1 \times 6}, O_{1 \times 3}]^T$, $\mathcal{M} = \left[\mathcal{T}(\alpha_0), \left. \frac{\partial}{\partial \alpha} (\mathcal{T}(\alpha) u) \right|_{\alpha_0, u_0}, -I \right]$, $\mathcal{Y} = \tau - \mathcal{T}(\alpha_0) u_0$, $\underline{\mathcal{U}} = [(\underline{u} - u_0)^T, \max((\underline{\alpha} - \alpha_0), \underline{\Delta\alpha})^T, \underline{o}^T]^T$, $\bar{\mathcal{U}} = [(\bar{u} - u_0)^T, \min((\bar{\alpha} - \alpha_0), \bar{\Delta\alpha})^T, \bar{o}^T]^T$.

C. LVIPDNN Optimization

To solve online the linear Quadratic Program (QP) problem shown in (77)-(78), a simplified gradient LVIPDNN is adopted. Firstly, the above optimization problem is converted

to the lagrangian dual problem. Follow [30], the dual problem is to maximize $\mathcal{H}(\mathcal{U})$ with

$$\begin{aligned} \mathcal{H}(\mathcal{U}) &= \inf\left\{\frac{1}{2} \mathcal{U}^T \mathcal{K} \mathcal{U} + \mathcal{W}^T \mathcal{U} + \mathcal{V}^T (\mathcal{Y} - \mathcal{M} \mathcal{U})\right. \\ &\quad \left. + \underline{\mathcal{L}}^T (\underline{\mathcal{U}} - \mathcal{U}) + \bar{\mathcal{L}}^T (\mathcal{U} - \bar{\mathcal{U}})\right\} \end{aligned} \quad (79)$$

where $\mathcal{V} \in \Omega_{\mathcal{V}}$, $\Omega_{\mathcal{V}} := \{\mathcal{V} \in \mathbb{R}^{3 \times 1} | -\bar{\mathcal{V}} \leq \mathcal{V} \leq \bar{\mathcal{V}}\}$. $\bar{\mathcal{V}}$ is a sufficiently large constant vector to represent $+\infty$. $\underline{\mathcal{L}}$ and $\bar{\mathcal{L}} \in \mathbb{R}^{6 \times 1}$ are dual-decision variables. The necessary and sufficient condition for a minimum is the vanishing of the gradient

$$\frac{\partial \mathcal{H}(\mathcal{U})}{\partial \mathcal{U}} = \mathcal{K} \mathcal{U} + \mathcal{W} - \mathcal{M}^T \mathcal{V} - \underline{\mathcal{L}} + \bar{\mathcal{L}} = 0 \quad (80)$$

With this condition, we can further obtain the following equation.

$$-\mathcal{U}^T \mathcal{K} \mathcal{U} = \mathcal{W}^T \mathcal{U} - \mathcal{V}^T \mathcal{M} \mathcal{U} - \underline{\mathcal{L}}^T \mathcal{U} + \bar{\mathcal{L}}^T \mathcal{U} \quad (81)$$

The dual quadratic formulation can be derived

$$J_d = \max\left\{-\frac{1}{2} \mathcal{U}^T \mathcal{K} \mathcal{U} + \mathcal{V}^T \mathcal{Y} + \underline{\mathcal{L}}^T \underline{\mathcal{U}} - \bar{\mathcal{L}}^T \bar{\mathcal{U}}\right\} \quad (82)$$

s.t. (80) with \mathcal{V} , $\underline{\mathcal{L}}$, $\bar{\mathcal{L}} \geq 0$. Our objective is to convert the QP problem into a set of LVIs by finding a primal-dual equilibrium vector $\mathcal{U}^* \in \Omega_{\mathcal{U}}$, $\mathcal{V} \in \Omega_{\mathcal{V}}$ [31], such that

$$(\mathcal{U} - \mathcal{U}^*)^T (\mathcal{K} \mathcal{U}^* + \mathcal{W} - \mathcal{M}^T \mathcal{V}^*) \geq 0 \quad (83)$$

Similarly, the LVIs for (78) is

$$(\mathcal{V} - \mathcal{V}^*)^T (\mathcal{M} \mathcal{U}^* - \mathcal{Y}) \geq 0 \quad (84)$$

Combining (83) and (84), the LVIs for the whole system can be rewritten as

$$\begin{aligned} &\left(\begin{bmatrix} \mathcal{U} \\ \mathcal{V} \end{bmatrix} - \begin{bmatrix} \mathcal{U}^* \\ \mathcal{V}^* \end{bmatrix} \right)^T \left(\begin{bmatrix} \mathcal{K} & -\mathcal{M}^T \\ \mathcal{M} & 0 \end{bmatrix} \begin{bmatrix} \mathcal{U}^* \\ \mathcal{V}^* \end{bmatrix} + \begin{bmatrix} \mathcal{W} \\ -\mathcal{Y} \end{bmatrix} \right) \\ &= (\mathcal{Z} - \mathcal{Z}^*)^T (\mathcal{E} \mathcal{Z}^* + \mathcal{S}) \geq 0 \end{aligned} \quad (85)$$

where $\mathcal{Z} = \begin{bmatrix} \mathcal{U} \\ \mathcal{V} \end{bmatrix} \in \Omega_{\mathcal{Z}} = \Omega_{\mathcal{U}} \times \Omega_{\mathcal{V}}$, $\mathcal{E} = \begin{bmatrix} \mathcal{K} & -\mathcal{M}^T \\ \mathcal{M} & 0 \end{bmatrix}$ and $\mathcal{S} = \begin{bmatrix} \mathcal{W} \\ -\mathcal{Y} \end{bmatrix}$. The following piecewise linear equation is applied to reformulate the above LVIs [15].

$$\mathcal{G}_{\Omega_{\mathcal{Z}}} (\mathcal{Z} - (\mathcal{E} \mathcal{Z} + \mathcal{S})) - \mathcal{Z} = 0 \quad (86)$$

where $\mathcal{G}_{\Omega_{\mathcal{Z}}}(\bullet)$ denotes the projection operator on $\Omega_{\mathcal{Z}}$ with the following definition.

$$\mathcal{G}_{\Omega_{\mathcal{Z}}}(\mathcal{B}) \begin{cases} \underline{\mathcal{B}}, & \text{if } \mathcal{B} < \underline{\mathcal{B}} \\ \mathcal{B}, & \text{if } \underline{\mathcal{B}} \leq \mathcal{B} \leq \bar{\mathcal{B}} \\ \bar{\mathcal{B}}, & \text{if } \mathcal{B} > \bar{\mathcal{B}} \end{cases} \quad (87)$$

The following dynamical system is developed for (86) according to dynamic-solver design approach [31] [32].

$$\dot{\mathcal{Z}} = \Gamma_{\mathcal{Z}} (I + \mathcal{E}^T) \{ \mathcal{G}_{\Omega_{\mathcal{Z}}} (\mathcal{Z} - (\mathcal{E} \mathcal{Z} + \mathcal{S})) - \mathcal{Z} \} \quad (88)$$

$\Gamma_{\mathcal{Z}} \in \mathbb{R}^{18 \times 18}$ is positive parameter used to tune the convergence rate [33].

Theorem 1: Assume the existence of optimal solution to the locally convex QP problem in (77)-(78). The output of the

search law (88) is globally exponentially convergent to the optimal solution \mathcal{U}^* .

VI. SIMULATION STUDY

In this section, a supply vessel replica-Cybership II in the marine control laboratory of Norwegian University of Science and Technology (NTNU) [34] is considered as the case study to evaluate the performance of the proposed control scheme.

A. Environmental Forces

1) *Wind Forces*: The wind force model is as presented in (7). The wind direction is along X_0 with the velocity of 16m/s. The peak of wind drag coefficients are selected as $[C_x, C_y, C_N]^T = [0.1, 0.14, 0.1]^T$.

2) *Wave Forces*: In this section, the wave forces indicate the wave-induced drift forces. These forces refer to the nonzero slowly varying components of the total wave-induced force. In this paper, we assume that the high-frequency components, i.e., the first-order wave-induced forces are filtered out by filters in advance and in DP system, no control is applied to handle the high-frequency motion. The model of wave drift forces are considered as follow [16].

$$\tau_{\text{wave}}^{[dof]} = \sum_{k=1}^N \rho_{\text{water}} g_v |F_{\text{wave}2}(\omega_k, \beta_r)| A_k^2 \cos(\omega_e(U, \omega_k, \beta_r)t + \epsilon_k) \quad (89)$$

where, $|F_{\text{wave}2}(\omega_k, \beta_r)|$ is the amplitude of the mean drift force. ω_k and β_r are wave frequencies and the angle between the heading of the vessel and the attack direction of the wave. The wave comes from the same direction with the wind, i.e, $\beta_{\text{wave}} = 0$. The calculation of $|F_{\text{wave}2}(\omega_k, \beta_r)|$ should be obtained by complex RAO analysis. For simplicity, we adopt a sinusoidal function to estimate it. A_k satisfies $\frac{1}{2}A_k^2 = S(\omega_k)\Delta\omega$. $S(\omega)$ is the JONSWAP wave spectrum. The dominant wave frequency is denoted as ω_o and $\omega_o = 6 \times 10^{-4}$ rad/s. The encounter frequency ω_e is defined as $\omega_e(U, \omega_o, \beta) = \left| \omega_o - \frac{\omega_o^2}{g_v} U \cos(\beta) \right|$. U is the total speed of the ship. ϵ_k is the random phase angle chosen within the range of $[-0.2, 0.2]$ rad/s.

In this simulation, we assume that during the beginning 10s, the sea is calm and the state becomes moderate at 10s, which triggers the rotation motion of the FPSO. While, because of the shielding effect, the large wave force starts to attack the AV at 150s. After that, the drift force increases gradually and the model (89) is activated to generate the force and moment.

B. Control System Simulation Study

In response to wind and wave force acting on the FPSO, the trajectory of FPSO is approximately a quarter round with the amplitude of 17m and frequency of 0.005rad/s. Thus,

the desired trajectory of the accommodation vessel can be expressed as

$$\begin{cases} \eta_{xd}(t) = 17\sin(0.005(t - t_m)) \\ \eta_{yd}(t) = -17\sin\left(0.005(t - t_m) + \frac{\pi}{2}\right) \\ \eta_{zd}(t) = \frac{\pi}{2} - \arctan\left(\frac{|\eta_{xd}|}{|\eta_{yd}|}\right) \end{cases} \quad (90)$$

where $t_m = 10s$ is the moment when the sea state changes. The initial position and velocity of the vessel are $\eta_0 = \left[0, -17, \frac{\pi}{2}\right]^T$ and $\nu_0 = [0, 0, 0]^T$. The total simulation time is 324s.

1) *Sea Observer*: Initially, (35) is applied to approximate the position and velocity of the vessel as well as the wind force and moment before alarm. The parameters are designed as $L = 5I_{6 \times 6}$, $C = I_{6 \times 6}$. Γ and P in adaptive law (21) are selected as $\Gamma = \text{diag}\{100, 600, 100\}$ and $P = 5I_{6 \times 6}$ respectively. The initial condition of the observer and the wind drag coefficient estimator are designed as $X_0 = [\eta_0, \nu_0]^T$ and $\hat{\Phi}_0 = [0.024, 0.056, 0.033]^T$.

Due to the effect of wave-induced force, when the vessel moves out of the shadow of the FPSO, the wind force estimator would conduct overcompensation. The overcompensation provide us with adequate hint to decide when the NN compensator is on. If the mean value of the estimated wind drag coefficients in past 5 successive seconds is above 0.2, a judgement can be made that severe wave force is attacking the vessel and the NN compensation needs to be activated both in the sea observer and in the controller.

After the compensation is triggered, since the overcompensated wind estimator cannot approximate the wave-induced forces perfectly, the update law with NN estimator (15) is applied. The network in this observer has 2^5 nodes. The inputs Z_{ow} contain $A_o, \omega_o, \beta_{\text{wave}}, \hat{\eta}_x, \hat{\eta}_y, \hat{\eta}_\phi$. Where A_o denotes A_k in (89) at the point of dominant frequency ω_o . The corresponding center are distributed in $[-0.5, 0.5]$, $[-0.5, 0.5]$, $[-0.5, 0.5]$, $[-0.5, 0.5]$, $[-0.5, 0.5]$ and $[-2, 2]$ respectively. The initial values of the weights are $\hat{W}_{di} = O_{2^5 \times 1}$, ($i = 1, 2, 3$). The updating rate in adaptive law (25) is $\omega_i = 0.002$, ($i = 1, 2, 3$).

2) *Robust Control*: Before the switching command is received from sea observer, dynamic model in (36) is considered. The input time delay t_d is 2s. The disturbance d is chosen randomly between -0.05-0.05. The gangway is able to rotate 360° freely, thus the tracking error constraint on yaw motion is relatively loose. N_b is set to be $N_b = \left[0.3, 0.3, \frac{\pi}{6}\right]^T$. Control law in (52) is applied with the parameters tuned as $K_1 = 0.001\text{diag}\{6, 6, 4\}$, $K_2 = 0.001\text{diag}\{6, 6, 4\}$, $\Gamma_1 = 0.001\text{diag}\{1, 1, 2\}$ and $\Theta = 0.001\text{diag}\{1, 1, 1\}$. The initial condition of the auxiliary state is $z_{f0} = [0, 0, 0]^T$.

When NN is required for wave force compensation, control law (66) is activated. The network also contains 2^5 nodes with the center evenly distributed in $[-0.5, 0.5]$, $[-0.5, 0.5]$, $[-0.5, 0.5]$, $[-0.5, 0.5]$, $[-0.5, 0.5]$ and $[-2, 2]$ respectively. The initial value of the weights are $\hat{W}_{ci} = O_{2^5 \times 1}$, ($i = 1, 2, 3$). The input of the network Z_c include $A_o, \omega_o, \beta_{\text{wave}}, \hat{\eta}_x, \hat{\eta}_y, \eta_\phi$. The updating rates in (65) are tuned as $\Upsilon_i = 2.2$ and

$\xi_i = 2.2$, ($i = 1, 2, 3$). The wind and wave forces and moment acting on the vessel can be found in Fig. (5). The control performance can be seen from Fig. (6)-(9).

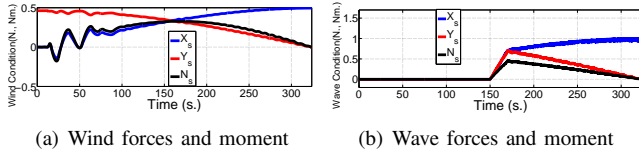


Fig. 5. Environmental forces and moment.

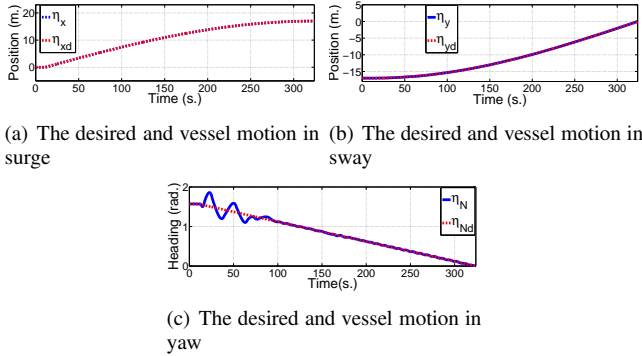


Fig. 6. Control performance in 3 DOFs.

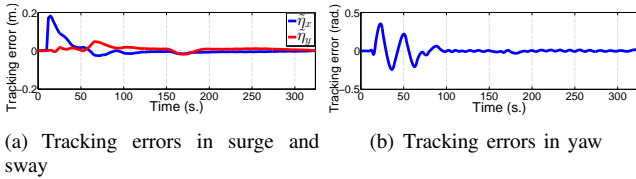


Fig. 7. Tracking errors.

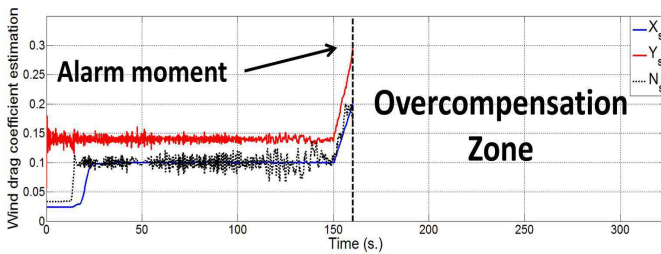


Fig. 8. Estimated wind drag coefficient

3) *Thrust Allocation*: The configuration of the six thrusters are shown in Fig. 3. The encounter angles $\alpha_{e2}, \alpha_{e3}, \alpha_{e4}$ and α_{e5} are defined in Fig. 10. The specific values of the encounter angles are calculated as $\alpha_{e2} = 190.9086^\circ$, $\alpha_{e3} = 191.5165^\circ$, $\alpha_{e4} = 10.8194^\circ$, $\alpha_{e5} = 11.5165^\circ$. Considering the forbidden zone of 20° , the working zone, in other words, the constraints for the azimuth angles are defined as $0^\circ \leq \alpha_1 \leq 360^\circ$, $0^\circ \leq \alpha_2 \leq 180.8194^\circ \cup 200.8194^\circ \leq \alpha_2 \leq 360^\circ$, $0^\circ \leq \alpha_3 \leq 181.5165^\circ \cup 201.5165^\circ \leq \alpha_3 \leq 360^\circ$, $0^\circ \leq \alpha_4 \leq 0.8194^\circ \cup 20.8194^\circ \leq \alpha_4 \leq 360^\circ$, $0^\circ \leq \alpha_5 \leq 1.5165^\circ \cup 21.5165^\circ \leq \alpha_5 \leq 360^\circ$, $0^\circ \leq \alpha_6 \leq 360^\circ$ For the

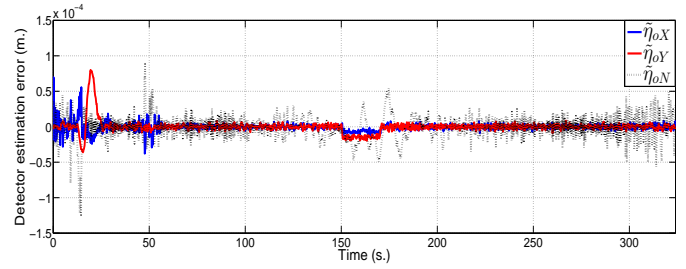


Fig. 9. State estimation error of the sea observer

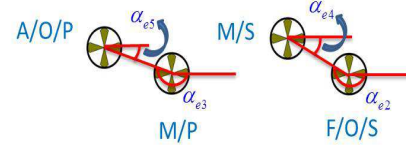


Fig. 10. Definition of encounter angle

ease of calculation, we need to merge the separated subset of $\alpha_2, \alpha_3, \alpha_4$ and α_5 into the following form.

$$\begin{aligned} 200.819^\circ \leq \alpha_2 \leq 540.819^\circ, 201.517^\circ \leq \alpha_3 \leq 541.517^\circ \\ 20.819^\circ \leq \alpha_4 \leq 360.819^\circ, 21.517^\circ \leq \alpha_5 \leq 361.517^\circ \end{aligned} \quad (91)$$

Particularly, since α_1 and α_6 can achieve full round rotation, in simulation, we set no constraint of rotation angle for α_1 and α_6 . The optimization weights \mathcal{Q} , \mathcal{P} and \mathcal{R} are selected as $\mathcal{Q} = 0.2I_{6 \times 6}$, $\mathcal{P} = 0.2I_{6 \times 6}$ and $\mathcal{R} = 10I_{3 \times 3}$. The updating parameter Γ_Z in the dynamic solver (88) is tuned as $\Gamma_Z = 0.1I_{18 \times 18}$. The upper and lower bound of the variables in (75-76) are $\underline{u} = -0.7\text{ones}(6, 1)$, $\bar{u} = 0.7\text{ones}(6, 1)$, $\underline{\Delta\alpha} = -\frac{\pi}{20}\text{ones}(6, 1)/\Delta t_{\text{opt}}$, $\bar{\Delta\alpha} = \frac{\pi}{20}\text{ones}(6, 1)/\Delta t_{\text{opt}}$. Where $\Delta t_{\text{opt}} = 0.167\text{s}$ is the sampling time interval between two loops. The constraint for the allocation error of the dynamic solver are $\underline{\rho} = -0.02\text{ones}(6, 1)$ and $\bar{\rho} = 0.02\text{ones}(6, 1)$. The initial thrust that each thruster provides are $u_0 = 0.0308\text{ones}(6, 1)$. The initial rotation angles are $\alpha_0 = \left[\frac{\pi}{2}, \frac{5\pi}{2}, \frac{5\pi}{2}, \frac{\pi}{2}, \frac{\pi}{2}, \frac{\pi}{2} \right]^T$. To reduce the computation consumption, in practical implementation, a termination mechanism is introduced for each optimization loop. The maximum iteration number in each loop is 10^5 . If the variance of J_C during the past 1000 successive iteration is smaller than 10^{-12} , the convergence of current loop can be rationally identified and computation process is terminated. Fig. (11)-(14) show the simulation results of the dynamic allocator.

C. Discussion

Figs. 6 shows that the proposed control can handle the input delay under severely varying environmental circumstances. Good tracking performance is achieved under the hybrid feedforward and feedback control scheme in surge and sway. However, there is relatively large oscillation at the beginning of tracking in yaw direction, but the heading angle is able to converge to the desired trajectory gradually. The corresponding

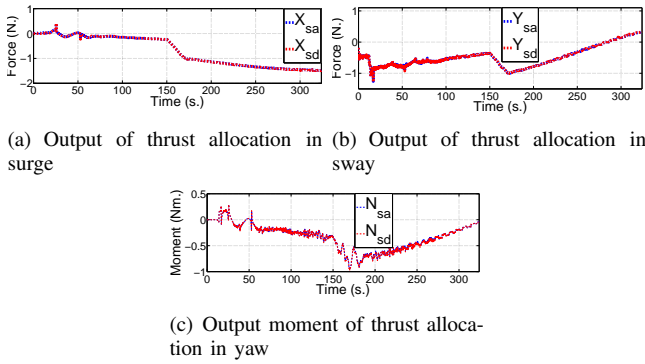


Fig. 11. Output of thrust allocation results.

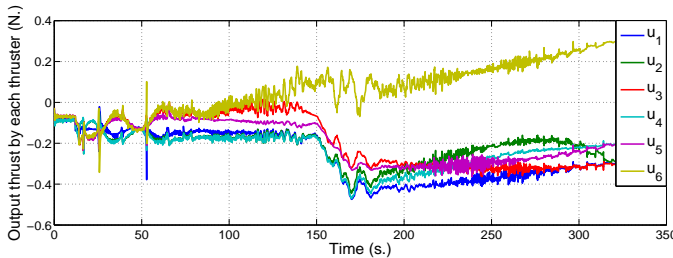


Fig. 12. Output thrust by each thruster

tracking errors are shown in Figs. 7. It can be observed that all the tracking errors are successfully restricted within the predefined constraint \tilde{N}_d . The estimation of the peak of wind drag coefficient $\tilde{\Phi}$ is presented in Fig. 8. As we can see, before the attack of the large wave-induced force, i.e. $t < 150s$, the estimator is able to achieve accurate approximation. After the attack, the estimation values start to increase rapidly which help to trigger the compensation. The alarm is activated at 160.17s. After the alarm, the estimation values fall in overcompensation and the simulation curves are ignored in the plot because they do not have adequate actual meaning. The observation error for plane position in the sea state observer is necessarily small as shown in Fig. 9. However, larger observation error can be seen during 150s-160s due to the effect of the wave force. The large observer error vanishes after the involvement the NN compensator. This abrupt error

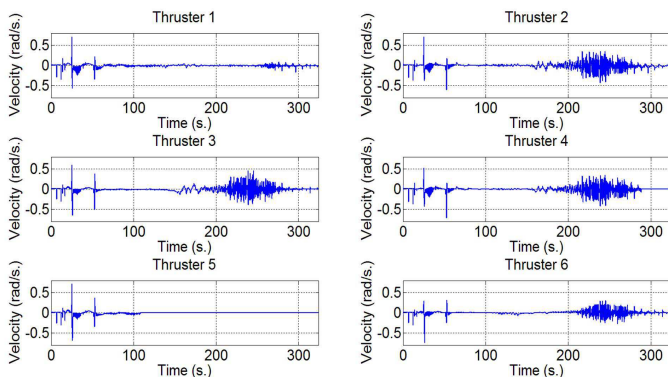


Fig. 13. Angular velocity of each thruster

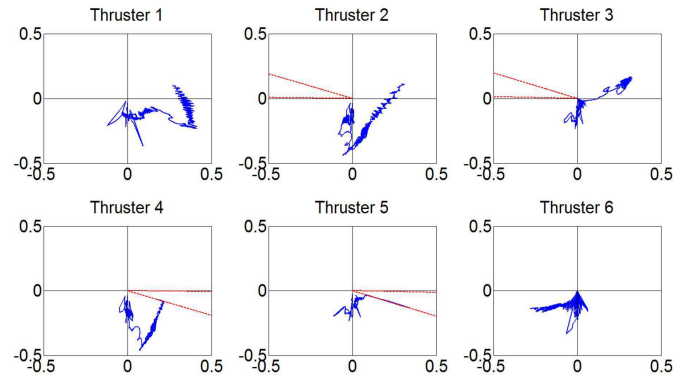


Fig. 14. Azimuth angle and output thrust tracking record

variation can be employed as an auxiliary indicator to decide the alarm moment.

In Figs. 11, the blue and red line represent the allocated generalized force and the command signal from the controller respectively. The results demonstrate that the dynamic allocator can provide satisfactory resulting force and moment to match the desired command signal. The produced thrust of each thruster is always within the limit of $\pm 0.7N$ as shown in Fig. 12. Combining Figs. 13-14, it is observed that constraints for the rotation angle and angular velocity are both not violated.

VII. CONCLUSION

In this paper, DP control has been proposed for a marine vessel under uncertain environmental force variation due to adjoining FPSO. First, a novel sea state observer has been developed with adaptive wind force and moment estimator to alarm large wave-induced drift force. Then, the control system has been designed using SBLF and predictor-based method in combination with NN to handle the tracking error constraints, input delay as well as the unknown wave force. The stability of the proposed sea state observer and the controller has been shown through rigorous Lyapunov and Lyapunov-Krasovskii analysis respectively. Finally, dynamic thrust allocation has been sequently investigated for individual thrusters of the DP system employing locally convex reformulation and LVIPDNN method. Simulation study has been conducted to verify the effectiveness of the proposed control scheme and thrust allocation.

REFERENCES

- [1] F. P. Rampazzo, J. L. B. Silva, D. P. Vieira, A. L. Pacifico, L. M. Junior, and E. A. Tannuri, "Numerical and experimental tools for offshore dp operations," in *ASME 2011 30th International Conference on Ocean, Offshore and Arctic Engineering*, pp. 685–692, American Society of Mechanical Engineers, 2011.
- [2] M. Van and H.-J. Kang, "Robust fault-tolerant control for uncertain robot manipulators based on adaptive quasi-continuous high-order sliding mode and neural network," *Proceedings of the Institution of Mechanical Engineers, Part C: Journal of Mechanical Engineering Science*, p. 0954406214544311, 2015.
- [3] M. Van, H.-J. Kang, Y.-S. Suh, and K.-S. Shin, "A robust fault diagnosis and accommodation scheme for robot manipulators," *International Journal of Control, Automation and Systems*, vol. 11, no. 2, pp. 377–388, 2013.

- [4] K. P. Tee, B. Ren, and S. S. Ge, "Control of nonlinear systems with time-varying output constraints," *Automatica*, vol. 47, no. 11, pp. 2511–2516, 2011.
- [5] C. P. Bechlioulis, G. Rovithakis, *et al.*, "Robust approximation free prescribed performance control," in *Control & Automation (MED), 2011 19th Mediterranean Conference on*, pp. 521–526, IEEE, 2011.
- [6] D. Zhao, F. Ding, L. Zhou, W. Zhang, and H. Xu, "Robust control of neutral system with time-delay for dynamic positioning ships," *Mathematical Problems in Engineering*, 2014.
- [7] N. Bekiaris-Liberis and M. Krstic, "Stabilization of linear strict-feedback systems with delayed integrators," *Automatica*, vol. 46, no. 11, pp. 1902–1910, 2010.
- [8] M. Jankovic, "Forwarding, backstepping, and finite spectrum assignment for time delay systems," *Automatica*, vol. 45, no. 1, pp. 2–9, 2009.
- [9] Q. Zhu, T. Zhang, and S. Fei, "Adaptive tracking control for input delayed mimo nonlinear systems," *Neurocomputing*, vol. 74, no. 1, pp. 472–480, 2010.
- [10] Q. Zhu, T. Zhang, and Y. Yang, "New results on adaptive neural control of a class of nonlinear systems with uncertain input delay," *Neurocomputing*, vol. 83, pp. 22–30, 2012.
- [11] H. Du, N. Zhang, and F. Naghdly, "Actuator saturation control of uncertain structures with input time delay," *Journal of Sound and Vibration*, vol. 330, no. 18, pp. 4399–4412, 2011.
- [12] T. Fossen, T. Johansen, *et al.*, "A survey of control allocation methods for ships and underwater vehicles," in *Control and Automation, 2006. MED'06. 14th Mediterranean Conference on*, pp. 1–6, IEEE, 2006.
- [13] T. A. Johansen, T. I. Fossen, and S. P. Berge, "Constrained nonlinear control allocation with singularity avoidance using sequential quadratic programming," *Control Systems Technology, IEEE Transactions on*, vol. 12, no. 1, pp. 211–216, 2004.
- [14] G. B. Dantzig, *Linear programming and extensions*. Princeton university press, 1998.
- [15] Y. Zhang and J. Wang, "A dual neural network for convex quadratic programming subject to linear equality and inequality constraints," *Physics Letters A*, vol. 298, no. 4, pp. 271–278, 2002.
- [16] T. I. Fossen, *Handbook of marine craft hydrodynamics and motion control*. John Wiley & Sons, 2011.
- [17] T. I. Fossen, *Guidance and control of ocean vehicles*, vol. 199. Wiley New York, 1994.
- [18] S. S. Ge and J. Zhang, "Neural-network control of nonaffine nonlinear system with zero dynamics by state and output feedback," *Neural Networks, IEEE Transactions on*, vol. 14, no. 4, pp. 900–918, 2003.
- [19] S. S. Ge, C. C. Hang, T. H. Lee, and T. Zhang, *Stable adaptive neural network control*, vol. 13. Springer Science & Business Media, 2013.
- [20] R. E. Kalman, "Lyapunov functions for the problem of lur'e in automatic control," *Proceedings of the National Academy of Sciences of the United States of America*, vol. 49, no. 2, p. 201, 1963.
- [21] S. S. Ge and C. J. Harris, *Adaptive neural network control of robotic manipulators*. World Scientific Publishing Co., Inc., 1998.
- [22] M. Chen, S. S. Ge, and B. Voon Ee How, "Robust adaptive neural network control for a class of uncertain mimo nonlinear systems with input nonlinearities," *Neural Networks, IEEE Transactions on*, vol. 21, no. 5, pp. 796–812, 2010.
- [23] Z. Artstein, "Linear systems with delayed controls: A reduction," *Automatic Control, IEEE Transactions on*, vol. 27, pp. 869–879, Aug 1982.
- [24] K. P. Tee, S. S. Ge, and E. H. Tay, "Barrier lyapunov functions for the control of output-constrained nonlinear systems," *Automatica*, vol. 45, no. 4, pp. 918–927, 2009.
- [25] M. S. De Queiroz, J. Hu, D. M. Dawson, T. Burg, and S. R. Donepudi, "Adaptive position/force control of robot manipulators without velocity measurements: Theory and experimentation," *Systems, Man, and Cybernetics, Part B: Cybernetics, IEEE Transactions on*, vol. 27, no. 5, pp. 796–809, 1997.
- [26] F. Mazenc and P. Bliman, "Backstepping design for time-delay nonlinear systems," *IEEE Transactions on Automatic Control*, vol. 51, no. 1, pp. 149–154, 2006.
- [27] S. S. Ge and C. Wang, "Direct adaptive nn control of a class of nonlinear systems," *Neural Networks, IEEE Transactions on*, vol. 13, no. 1, pp. 214–221, 2002.
- [28] K. P. Tee and S. S. Ge, "Control of fully actuated ocean surface vessels using a class of feedforward approximators," *Control Systems Technology, IEEE Transactions on*, vol. 14, no. 4, pp. 750–756, 2006.
- [29] Y. Wei, M. Fu, J. Ning, and X. Sun, "Quadratic programming thrust allocation and management for dynamic positioning ships," *TELKOMNIKA Indonesian Journal of Electrical Engineering*, vol. 11, no. 3, pp. 1632–1638, 2013.
- [30] M. S. Bazaraa, H. D. Sherali, and C. M. Shetty, *Nonlinear programming: theory and algorithms*. John Wiley & Sons, 2013.
- [31] Y. Zhang, S. S. Ge, and T. H. Lee, "A unified quadratic-programming-based dynamical system approach to joint torque optimization of physically constrained redundant manipulators," *Systems, Man, and Cybernetics, Part B: Cybernetics, IEEE Transactions on*, vol. 34, no. 5, pp. 2126–2132, 2004.
- [32] Y. Zhang, Z. Tan, Z. Yang, X. Lv, and K. Chen, "A simplified lvi-based primal-dual neural network for repetitive motion planning of pa10 robot manipulator starting from different initial states," in *Neural Networks, 2008. IJCNN 2008. (IEEE World Congress on Computational Intelligence). IEEE International Joint Conference on*, pp. 19–24, IEEE, 2008.
- [33] Z. Li, S. S. Ge, and S. Liu, "Contact-force distribution optimization and control for quadruped robots using both gradient and adaptive neural networks," 2014.
- [34] R. Skjetne, T. I. Fossen, and P. V. Kokotović, "Adaptive maneuvering, with experiments, for a model ship in a marine control laboratory," *Automatica*, vol. 41, no. 2, pp. 289–298, 2005.

